

LC-PHSM-2003-071  
August 2003

# Study of Sleptons at a Linear Collider – Supersymmetry Scenario SPS 1a\*

Hans-Ulrich Martyn<sup>†</sup>

*I. Physikalisches Institut, RWTH Aachen, Germany*

The properties of the light charged sleptons in  $\tilde{e}_R \tilde{e}_R$ ,  $\tilde{\mu}_R \tilde{\mu}_R$  and  $\tilde{\tau}_1 \tilde{\tau}_1$  production are studied within the mSUGRA scenario SPS 1a. Various method are presented to determine very precisely masses, angular distributions, spin and couplings as well as the  $\tilde{\tau}_1$  polarisation and mixing parameter in the  $\tilde{\tau}$  sector. The analysis is based on a complete simulation of signal and background reactions assuming experimental conditions of the TESLA  $e^+e^-$  Linear Collider.

## 1 Introduction

This note describes, for a particular bench mark model, how masses and couplings of scalar leptons can be accurately measured at a future  $e^+e^-$  linear collider TESLA [1]. Beam conditions are chosen such as to stay below production thresholds of the heavier sleptons, the assumed luminosity corresponds to about one year of running at design parameters. Details of the experimental simulation, analysis and background information on kinematics and theory are given in sketchy form.

**Particle spectrum** mSUGRA SPS 1a scenario [2] (parameters  $m_0 = 100$  GeV,  $m_{1/2} = 250$  GeV,  $A_0 = -100$  GeV,  $\tan \beta = 10$ , sign  $\mu +$ ) shown in fig. 1. Cascade decays of  $\tilde{\chi}_2^0$ ,  $\tilde{\chi}_1^\pm$  lead to abundant  $\tau$  final states.

**Event generation** PYTHIA 6.2 [3] including beam polarisations  $\mathcal{P}_{e^\pm}$ , QED radiation, beamstrahlung à la CIRCE [4],  $\tau$  decays and  $\tau$  polarisation treated by TAUOLA [5]

---

\*Contribution to the Extended ECFA/DESY Study on Physics and Detectors for a Linear Electron-Positron Collider (2001 – 2003)

<sup>†</sup>email: martyn@mail.desy.de

**Operating conditions**  $\sqrt{s} = 400$  GeV, beam polarisations  $\mathcal{P}_{e^-} = +0.80$ ,  $\mathcal{P}_{e^+} = -0.60$ , integrated luminosity  $\mathcal{L} = 200 \text{ fb}^{-1}$   
 $\Rightarrow$  efficient suppression of SUSY ( $\tilde{\nu}_l$ ,  $\tilde{\chi}_2^0$ ,  $\tilde{\chi}_1^\pm$ ) and SM background

**Detector à la TDR [1]** Simulation based on SIMDET 4.02 [6], acceptance  $\theta > 125$  mrad,  $e, \gamma$  veto  $\theta > 4.6$  mrad

### Slepton production

$$e_L^+ e_R^- \rightarrow \tilde{\mu}_R \tilde{\mu}_R \quad (120 \text{ fb}) \quad (1)$$

$$e_L^+ e_R^- \rightarrow \tilde{e}_R \tilde{e}_R \quad (550 \text{ fb}) \quad (2)$$

$$e_L^+ e_R^- \rightarrow \tilde{\tau}_1 \tilde{\tau}_1 \quad (140 \text{ fb}) \quad (3)$$

**Background production** SUSY bkg  $e_L^+ e_R^- \rightarrow \tilde{e}_R \tilde{e}_L$  (75 fb),  $\tilde{\chi}_2^0 \tilde{\chi}_1^0$  (20 fb),  $\tilde{\chi}_1^+ \tilde{\chi}_1^+$  (5 fb)  
SM bkg  $e_L^+ e_R^- \rightarrow W^+ W^-$  (1000 fb) [ $B_{W \rightarrow \ell\nu} = 0.107$ ],  $e^+ e^- \rightarrow \ell^+ \ell^- (\gamma)$  negligible  
 $\gamma\gamma$  bkg negligible  $\sigma(e^+ e^- \rightarrow e^+ e^- \tau^+ \tau^-) = 4.5 \cdot 10^5 \text{ fb}$ , acceptance < few  $10^{-6}$

### Slepton decays

$$\tilde{\ell}^- \rightarrow \ell^- \tilde{\chi}_1^0 \quad (4)$$

Flat lepton energy spectrum with endpoints  $E_{+-}$  related to slepton and neutralino masses

$$E_{+-} = \frac{\sqrt{s}}{4} \left( 1 - \frac{m_{\tilde{\chi}}^2}{m_{\tilde{\ell}}^2} \right) (1 \pm \beta) \quad (5)$$

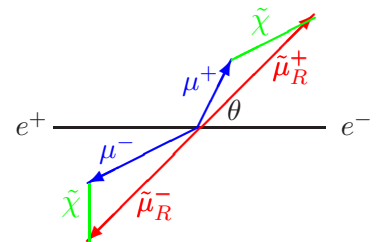
$$m_{\tilde{\ell}} = \frac{\sqrt{s}}{E_- + E_+} \sqrt{E_- E_+} \quad (6)$$

$$m_{\tilde{\chi}} = m_{\tilde{\ell}} \sqrt{1 - \frac{E_- + E_+}{\sqrt{s}/2}} \quad (7)$$

### $\ell^+ \ell^-$ momentum correlations [7]

$m_{\tilde{\chi}^0}$  known: energy-momentum conservation constrains construction of kinematically allowed minimum mass  $m_{\min}(\tilde{\ell})$   
sharp peak around true mass  $m_{\tilde{\ell}}$

$m_{\tilde{\chi}^0}$  and  $m_{\tilde{\ell}}$  known: reconstruct  $\tilde{\ell}$  direction  $\theta$   
two-fold ambiguity, false solution flat in  $\cos \theta$



## 2 Properties of smuons

**Selection criteria**  $e_L^+ e_R^- \rightarrow \tilde{\mu}_R \tilde{\mu}_R$  at  $\sqrt{s} = 400$  GeV

nr	cut	min	max	eff
0.	n_ch, n_gamma in accept.	2	0	0.815
	n_charge in acceptance	2	2	0.989
	n_gamma in acceptance	5.0	0	0.851
	n_veto in acceptance	5.0	0	0.960
1.	Q*cos_theta_l	-0.900	0.750	0.693
2.	delta phi_(l+,l-) (deg)		160.0	0.555
4.	p_T event (GeV)	10.0		0.553
5.	p_miss cos_theta_(l+l-)		0.900	0.537
7.	lepton energy (GeV)	2.5	150.0	0.537
10.	m_recoil + 0.4*m_ll (GeV)	240.0		0.537
efficiency		0.5365		
lepton energy E_min 16.52		E_max 93.30		

**Mass determination** Spectra of the muon energy  $E_\mu$  and minimum mass  $m_{\min}(\tilde{\mu}_R)$  are shown in fig. 2. The endpoint energies,  $E_- = 16.570 \pm 0.040$  GeV and  $E_+ = 93.30 \pm 0.22$  GeV, give strongly correlated  $\tilde{\mu}_R$  and  $\tilde{\chi}_1^0$  masses. The reconstructed masses from both methods agree well with the input values.

method	$m_{\tilde{\mu}_R}$ [GeV]	$m_{\tilde{\chi}_1^0}$ [GeV]
$E_\mu$ spectrum	$143.15 \pm 0.17$	$96.10 \pm 0.21$
$m_{\min}(\tilde{\mu}_R)$ spectrum	$142.98 \pm 0.03$	fixed
SPS 1a input	143.0	96.0

**Spin  $J = 0$  of  $\tilde{\mu}_R$**  The polar angle distribution of  $\tilde{\mu}_R \tilde{\mu}_R$  production is presented in fig. 3. After background subtraction on finds the typical cross section dependence

$$\frac{d\sigma}{d \cos \theta} \propto \sin^2 \theta$$

as expected for a scalar particle.

## 3 Properties of selectrons

**Selection criteria**  $e_L^+ e_R^- \rightarrow \tilde{e}_R \tilde{e}_R$  at  $\sqrt{s} = 400$  GeV

nr	cut	min	max	eff
0.	n_ch, n_gamma in accept.	2	0	0.742
	n_charge in acceptance	2	2	0.984
	n_gamma in acceptance	5.0	0	0.780
	n_veto in acceptance	5.0	0	0.960

```

1. Q*cos_theta_1           -0.900   0.750   0.586
2. delta phi_(l+,l-) (deg)    160.0   0.484
4. p_T event (GeV)          10.0    0.484
5. p_miss cos_theta_(l+l-)    0.900   0.468
7. lepton energy (GeV)        2.5    0.468
10. m_recoil + 0.4*m_ll (GeV) 240.0   0.468

efficiency      0.4675

lepton energy E_min 16.52      E_max 93.30

```

**Mass determination** Spectra of the electron energy  $E_e$  and minimum mass  $m_{\min}(\tilde{e}_R)$  are shown in fig. 4. The endpoint energies,  $E_- = 16.528 \pm 0.020$  GeV and  $E_+ = 93.34 \pm 0.11$  GeV, give strongly correlated  $\tilde{e}_R$  and  $\tilde{\chi}_1^0$  masses. The reconstructed masses from both methods are in agreement with the input values.

method	$m_{\tilde{e}_R}$ [GeV]	$m_{\tilde{\chi}_1^0}$ [GeV]
<b><math>E_e</math> spectrum</b>	$142.99 \pm 0.08$	$96.05 \pm 0.10$
<b><math>m_{\min}(\tilde{e}_R)</math> spectrum</b>	$142.97 \pm 0.02$	<b>fixed</b>
<b>SPS 1a input</b>	<b>143.0</b>	<b>96.0</b>

**Angular distribution of  $\tilde{e}_R$**  The polar angle distribution of  $\tilde{e}_R \tilde{e}_R$  production is presented in fig. 5. After background subtraction on finds the typical behaviour of  $t$ -channel neutralino exchange, given by the approximate matrix element

$$\mathcal{M} \sim \beta \sin \theta \left[ 1 - \frac{4 Y_{\tilde{B}}^2}{1 - 2 \beta \cos \theta + \beta^2 + 4 M_1^2/s} \right].$$

The differential cross section can be used to determine the Yukawa coupling  $Y_{\tilde{B}} = \hat{g}'_{\tilde{B}\tilde{e}e}/g'_{\gamma ee}$  and the gaugino mass parameter  $M_1$  at the percent level.

**Chiral quantum numbers** A unique determination of the selectron  $L/R$  quantum numbers is offered by the reaction  $e^+ e^- \rightarrow \tilde{e}_R \tilde{e}_L$ , which proceed via pure  $t$ -channel  $\tilde{\chi}^0$  exchange. The ‘chiral flow’ at the  $e \tilde{\chi}^0 \tilde{e}$  vertex associates the incoming electron/positron with its superpartner:  $e_L^- \rightarrow \tilde{e}_L^-$ ,  $e_R^- \rightarrow \tilde{e}_R^-$  and  $e_L^+ \rightarrow \tilde{e}_R^+$ ,  $e_R^+ \rightarrow \tilde{e}_L^+$ . Measuring the energy spectra of the decay  $e^-$  and  $e^+$  separately allows for a clear distinction between  $\tilde{e}_R$  and  $\tilde{e}_L$ . Moreover, by choosing appropriate beam polarisations, *e.g.* ‘odd’ combinations  $e_R^+ e_L^- \rightarrow \tilde{e}_L^+ \tilde{e}_R^-$  or  $e_L^+ e_L^- \rightarrow \tilde{e}_R^+ \tilde{e}_L^-$ , one suppresses the  $s$ -channel  $\gamma, Z$  amplitudes of  $\tilde{e}_R \tilde{e}_R$  and other background and enhances the  $\tilde{e}_R \tilde{e}_L$  production considerably, as illustrated in fig. 6 and fig. 7. Contributions from  $\tilde{e}_R \tilde{e}_R$  are identical in both  $e^\pm$  spectra and can be readily subtracted since  $m_{\tilde{e}_R}$  is known. A measurement of the  $\tilde{e}_L$  mass of  $m_{\tilde{e}_L} = 202.1 \pm 0.5$  GeV appears feasible. Similar studies are reported in [8].

## 4 Properties of staus

**Parameters**  $L - R$  mixing in third generation, access to  $\tan \beta$  and  $A_\tau$  [9, 10]

$$\begin{pmatrix} \tilde{\tau}_1 \\ \tilde{\tau}_2 \end{pmatrix} = \begin{pmatrix} \cos \theta_{\tilde{\tau}} & \sin \theta_{\tilde{\tau}} \\ -\sin \theta_{\tilde{\tau}} & \cos \theta_{\tilde{\tau}} \end{pmatrix} \begin{pmatrix} \tilde{\tau}_L \\ \tilde{\tau}_R \end{pmatrix} \quad (8)$$

$$\tan 2 \theta_{\tilde{\tau}} = \frac{-2 m_\tau (A_\tau - \mu \tan \beta)}{m_{\tilde{\tau}_R}^2 - m_{\tilde{\tau}_L}^2} \quad (9)$$

$\tau$  polarisation  $\mathcal{P}_\tau$  in decay  $\tilde{\tau}_1 \rightarrow \tau \tilde{\chi}_1^0$        $\mathcal{P}_\tau = \mathcal{P}_\tau(\theta_{\tilde{\tau}}, \tan \beta, \tilde{\chi}_1^0$  mixing)

**Selection criteria**  $e_L^+ e_R^- \rightarrow \tilde{\tau}_1^+ \tilde{\tau}_1^-$  at  $\sqrt{s} = 400$  GeV

nr	cut	min	max	eff			
0.	n_charge, n_veto	2	6	0.931			
1.	n_jets		2	0.834			
2.	n_taus		2	0.829			
3.	n_leptons		0	0.780			
4.	E_jet (GeV)		2.5	0.739			
5.	Q*cos_theta_jet	-0.950	0.750	0.597			
8.	mass tau_jet (GeV)		2.000	0.547			
11.	delta phi_(l, di-jet) (deg)		160.0	0.426			
12.	cos theta_P_miss		0.95	0.424			
13.	p_T (GeV)	10.0	200.0	0.400			
efficiency SUSY							
0.3999							
tau decay statistics							
		e	mu	pi	rho	3_pi	sum
e	0	510	529	1097	1125	3261	
mu	0	0	470	1040	1121	2631	
pi	0	0	200	783	819	1802	
rho	0	0	0	821	1786	2607	
3_pi	0	0	0	0	895	895	
sum	0	510	1199	3741	5746	11196	
lepton energy					E_min	12.19	
					E_max	83.81	

Leptonic  $\tau$  decays not useful and discarded due to large  $WW$  background

Analysed decay modes & branching ratios

$$\mathcal{B}(\tau \rightarrow \pi \nu_\tau) = 0.111, \mathcal{B}(\tau \rightarrow \rho \nu_\tau) = 0.254, \mathcal{B}(\tau \rightarrow 3\pi \nu_\tau) = 0.194$$

**$m_{\tilde{\tau}_1}$  from  $\tau$  decays**  $\tau \rightarrow \rho \nu_\tau \rightarrow \pi^\pm \pi^0 \nu_\tau$  and  $\tau \rightarrow 3\pi \nu_\tau \rightarrow \pi^\pm \pi^\pm \pi^\mp \nu_\tau + \pi^\pm \pi^0 \pi^0 \nu_\tau$   
 $E_\rho, E_{3\pi}$  sensitive to  $m_{\tilde{\tau}_1}$ , almost independent of  $\mathcal{P}_\tau$

Analysis of  $E_\rho$  and  $E_{3\pi}$  spectra, shown in fig. 8, assuming  $m_{\tilde{\chi}_1^0}$  known

mode	$m_{\tilde{\tau}_1}$ [GeV]
$E_\rho$	$133.3 \pm 0.75$
$E_{3\pi}$	$133.2 \pm 0.30$
mean	$133.2 \pm 0.30$
SPS 1a input	133.2

**$\theta_{\tilde{\tau}}$  from cross section** A cross section measurement of  $\sigma_{\tilde{\tau}_1 \tilde{\tau}_1} = 137.8 \pm 2.2_{\text{stat}} \pm 1.4_{\text{sys}} \text{ fb}$  (incl. ISR & BS) provides a  $\tilde{\tau}$  mixing angle of  $\cos 2 \theta_{\tilde{\tau}} = -0.84 \pm 0.04$ , see fig. 10

**$\tau$  polarisation  $\mathcal{P}_\tau$**   $E_\pi$  from  $\tau \rightarrow \pi \nu_\tau$  and  $z_\pi = E_\pi/E_\rho$  from  $\tau \rightarrow \rho \nu_\tau \rightarrow \pi \pi^0 \nu_\tau$   $E_\pi, z_\pi$  sensitive to  $\mathcal{P}_\tau$ , almost independent of  $m_{\tilde{\tau}_1}$

$\tau$  is self-analysing system – spin correlations

$\tau_R^- \rightarrow \pi^- \nu$	$\mathcal{P}_\tau = +1$	$\pi^-$ emitted in forward direction	$E_\pi \nearrow$
$\tau_L^- \rightarrow \pi^- \nu$	$\mathcal{P}_\tau = -1$	$\pi^-$ emitted in backward direction	$E_\pi \searrow$
$\tau_R^- \rightarrow \rho_L^- \nu$	$\mathcal{P}_\tau = +1$	$d\sigma/dz_\pi \propto (2z_\pi - 1)^2$	asymmetric sharing $z_\pi \rightarrow 0 / 1$
$\tau_L^- \rightarrow \rho_T^- \nu$	$\mathcal{P}_\tau = -1$	$d\sigma/dz_\pi \propto 2z_\pi(1 - z_\pi)$	equal sharing $z_\pi \rightarrow 0.5$

Analysis of  $E_\pi$  and  $z_\pi$  spectra, shown in fig. 9,  $m_{\tilde{\chi}_1^0}$  assumed to be known

mode	$\mathcal{P}_\tau$
$E_\pi$	$0.98 \pm 0.045$
$z_\pi = E_\pi/E_\rho$	$1.02 \pm 0.038$
mean	$1.00 \pm 0.035$
SPS 1a input	0.981

A polarisation measurement of  $\mathcal{P}_\tau = 1.00 \pm 0.035$  is not sensitive enough to determine  $\tan \beta$  in SPS 1a, where one has  $\delta \mathcal{P}_\tau / \delta \tan \beta = 0.3\%$

## 5 Summary

Simulations of slepton production  $e^+ e^- \rightarrow \tilde{e}_R \tilde{e}_R, \tilde{\mu}_R \tilde{\mu}_R, \tilde{\tau}_1 \tilde{\tau}_1$  in the SPS 1a mSUGRA scenario under realistic experimental conditions assuming  $\sqrt{s} = 400 \text{ GeV}, \mathcal{L} = 200 \text{ fb}^{-1}$  and beam polarisations  $\mathcal{P}_{e^-} = +0.8, \mathcal{P}_{e^+} = -0.6$  are presented. The slepton and neutralino  $\tilde{\chi}_1^0$  masses as well as the polarisation  $\mathcal{P}_{\tilde{\tau}_1 \rightarrow \tau \tilde{\chi}_1^0}$  and mixing parameter  $\theta_{\tilde{\tau}}$  of the third generation can be accurately determined with moderate integrated luminosity. Improvements on  $m_{\tilde{e}_R}$  and  $m_{\tilde{\mu}_R}$  are possible if  $\delta m_{\tilde{\chi}_1^0}$  can be reduced, *e.g.* by studying neutralino production and decays. An alternative method to measure selectron and smuon masses via cross section threshold scans is discussed in [11]. Other estimates on SPS 1a sparticle masses can be found in [8] and [12] (not based on detailed simulations).

$\tilde{e}_R$	$m_{\tilde{e}_R} = 142.99 \pm 0.08 \text{ GeV}$	$m_{\tilde{\chi}_1^0} = 96.05 \pm 0.10 \text{ GeV}$
$\tilde{\mu}_R$	$m_{\tilde{\mu}_R} = 143.15 \pm 0.17 \text{ GeV}$	$m_{\tilde{\chi}_1^0} = 96.10 \pm 0.21 \text{ GeV}$
$\tilde{\tau}_1$	$m_{\tilde{\tau}_1} = 133.2 \pm 0.30 \text{ GeV}$	—
	$\cos 2 \theta_{\tilde{\tau}} = -0.84 \pm 0.04$	$\mathcal{P}_\tau = 1.00 \pm 0.035$

**Acknowledgement** I want to thank G. Moortgat-Pick for the stimulating discussions on the stau sector and for providing the plot of fig. 10.

## References

- [1] TESLA Technical Design Report, DESY 2001-011, Part III: *Physics at an  $e^+e^-$  Linear Collider* [hep-ph/0106315], Part IV: *A Detector for TESLA*.
- [2] B.C. Allanach et al., Eur. Phys. J. C 25 (2002) 113;  
N. Ghodbane, H.-U. Martyn, hep-ph/0201233.
- [3] PYTHIA, T. Sjöstrand et al., Comput. Phys. Commun. 135 (2001) 238.
- [4] CIRCE, T. Ohl, Comput. Phys. Commun. 101 (1997) 269.
- [5] TAUOLA, S. Jadach et al., Comput. Phys. Commun. 76 (1993) 361.
- [6] SIMDET, M. Pohl, J. Schreiber, DESY-02-061, hep-ex/0206009.
- [7] J. Feng, D. Finell, Phys. Rev. D 49 (1994) 2369.
- [8] M. Dima et al., Phys. Rev. D 65 (2002) 71701.
- [9] M.M. Nojiri, Phys. Rev. D 51 (1995) 6281;  
M.M. Nojiri, K. Fujii, T. Tsukamoto, Phys. Rev. D 54 (1996) 6756.
- [10] E. Boos et al., Eur. Phys. J. C 30 (2003) 395.
- [11] A. Freitas, A. von Manteuffel, proceedings SUSY 02, DESY Hamburg, Germany, 2002, hep-ph/0211105.
- [12] P. Grannis, talk at LCWS 02, Jeju Island, Korea, 2002, hep-ex/0211002.

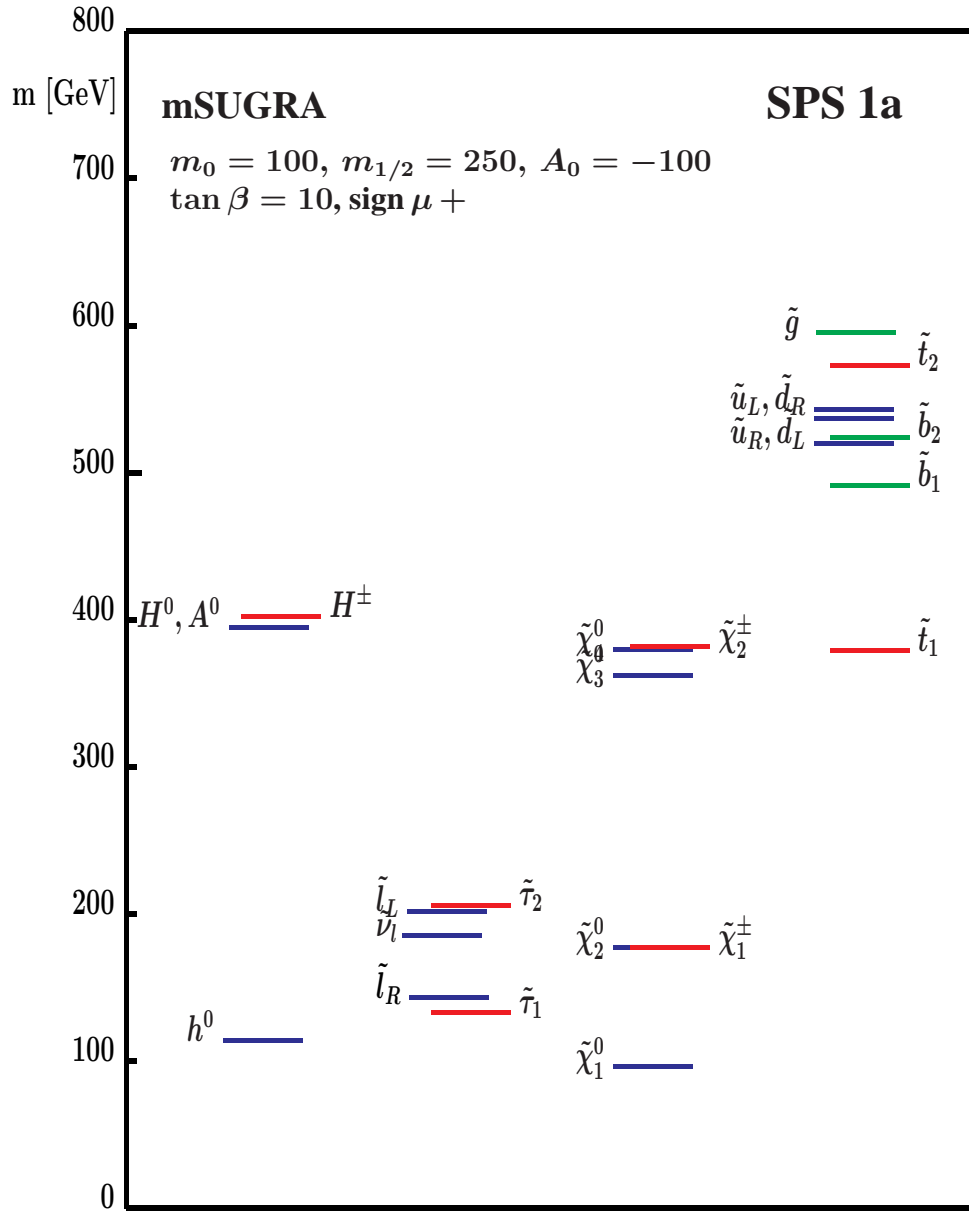


Figure 1: Particle spectrum of mSUGRA benchmark scenario SPS 1a

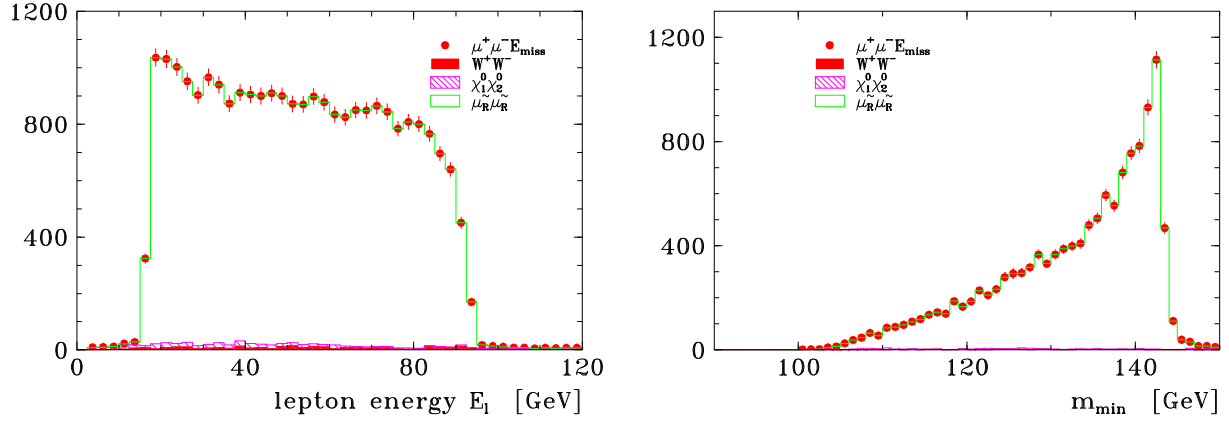


Figure 2: Energy spectrum  $E_\mu$  of muons (left) and minimum mass  $m_{\min}(\tilde{\mu}_R)$  (right) from the reaction  $e_L^+ e_R^- \rightarrow \tilde{\mu}_R^+ \tilde{\mu}_R^- \rightarrow \mu^+ \tilde{\chi}_1^0 \mu^- \tilde{\chi}_1^0$ ; mSUGRA model SPS 1a at  $\sqrt{s} = 400$  GeV and  $\mathcal{L} = 200 \text{ fb}^{-1}$

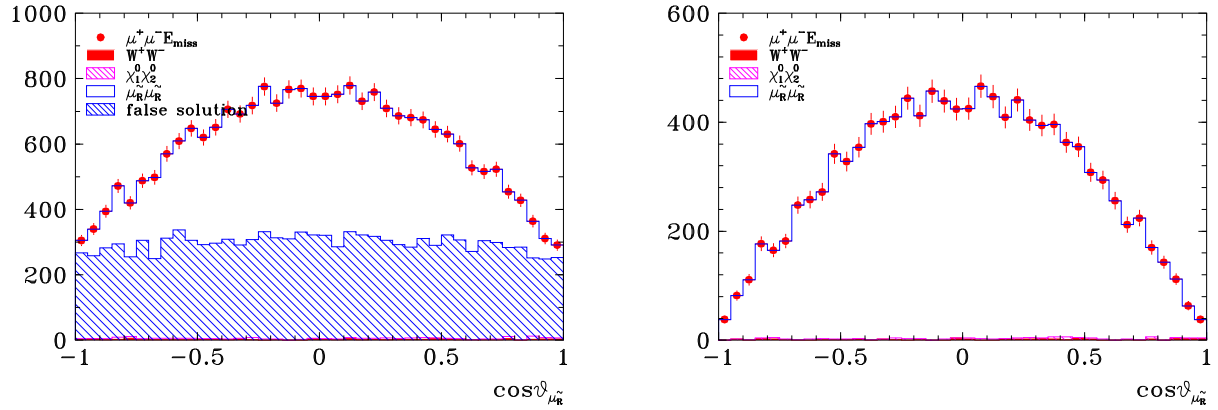


Figure 3: Polar angle distribution of  $\tilde{\mu}_R$  with (left) and without (right) contribution of false solution in the reaction  $e_L^+ e_R^- \rightarrow \tilde{\mu}_R^+ \tilde{\mu}_R^- \rightarrow \mu^+ \tilde{\chi}_1^0 \mu^- \tilde{\chi}_1^0$ ; mSUGRA model SPS 1a at  $\sqrt{s} = 400$  GeV and  $\mathcal{L} = 200 \text{ fb}^{-1}$

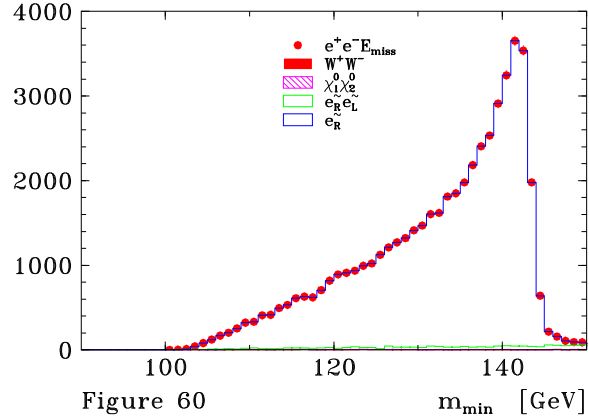
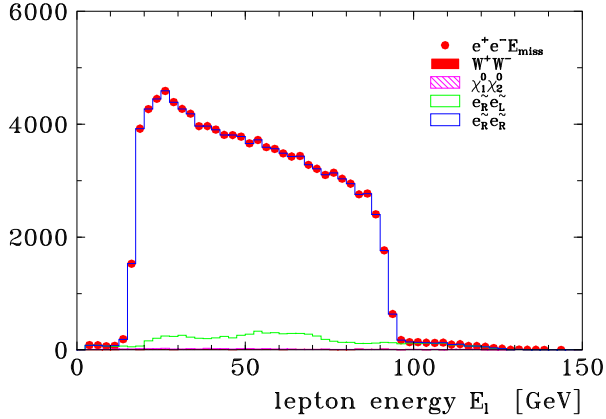


Figure 4: Energy spectrum  $E_e$  of electrons (left) and minimum mass  $m_{\min}(\tilde{e}_R)$  (right) from the reaction  $e_L^+ e_R^- \rightarrow \tilde{e}_R^+ \tilde{e}_R^- \rightarrow e^+ \tilde{\chi}_1^0 e^- \tilde{\chi}_1^0$ ; mSUGRA model SPS 1a at  $\sqrt{s} = 400$  GeV and  $\mathcal{L} = 200 \text{ fb}^{-1}$

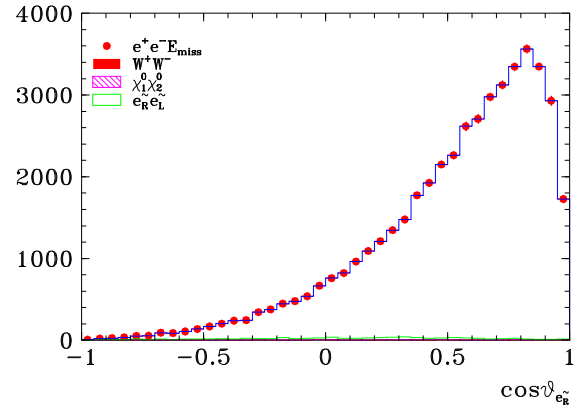
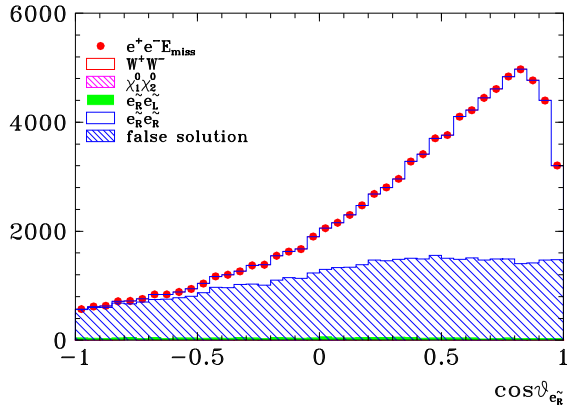
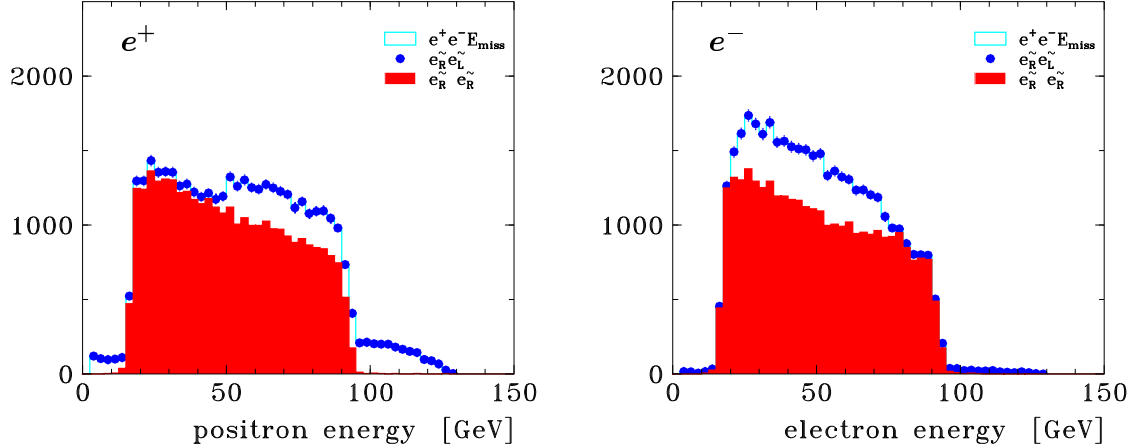
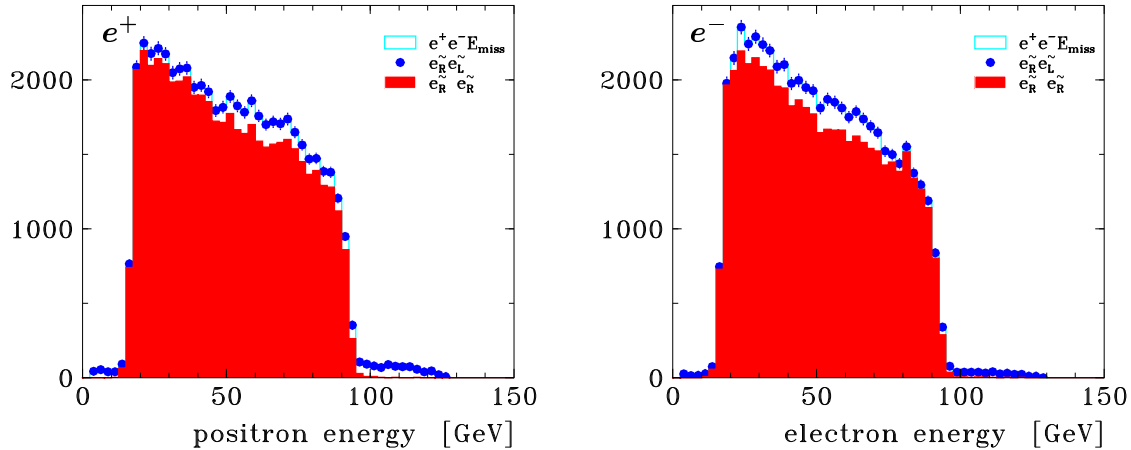


Figure 5: Polar angle distribution of  $\tilde{e}_R$  with (left) and without (right) contribution of false solution in the reaction  $e_L^+ e_R^- \rightarrow \tilde{e}_R^+ \tilde{e}_R^- \rightarrow e^+ \tilde{\chi}_1^0 e^- \tilde{\chi}_1^0$ ; mSUGRA model SPS 1a at  $\sqrt{s} = 400$  GeV and  $\mathcal{L} = 200 \text{ fb}^{-1}$

$$e^+ e^- \rightarrow \tilde{e}_R \tilde{e}_R, \tilde{e}_R \tilde{e}_L$$



$$e^+_L e^-_R \rightarrow \tilde{e}_R \tilde{e}_R, \tilde{e}_R \tilde{e}_L$$



$$e^+_R e^-_R \rightarrow \tilde{e}_R \tilde{e}_R, \tilde{e}_R \tilde{e}_L$$

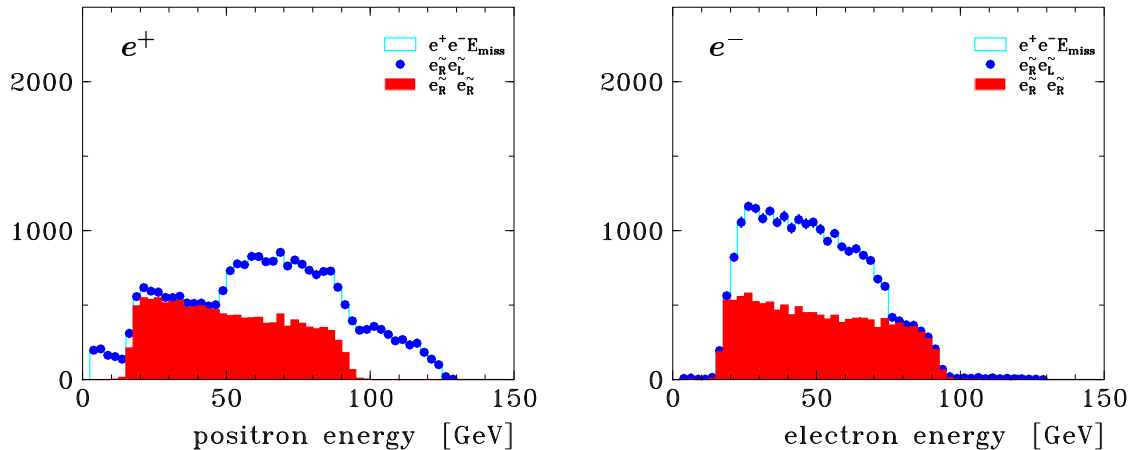


Figure 6:  $e^\pm$  energy spectra from  $e^+ e^- \rightarrow \tilde{e}_R \tilde{e}_R + \tilde{e}_R \tilde{e}_L$  production with polarisations  $\mathcal{P}_{e^-} = +0.8$ ,  $\mathcal{P}_{e^+}$  variable for SPS 1a scenario assuming  $\sqrt{s} = 400$  GeV and  $\mathcal{L} = 200 \text{ fb}^{-1}$

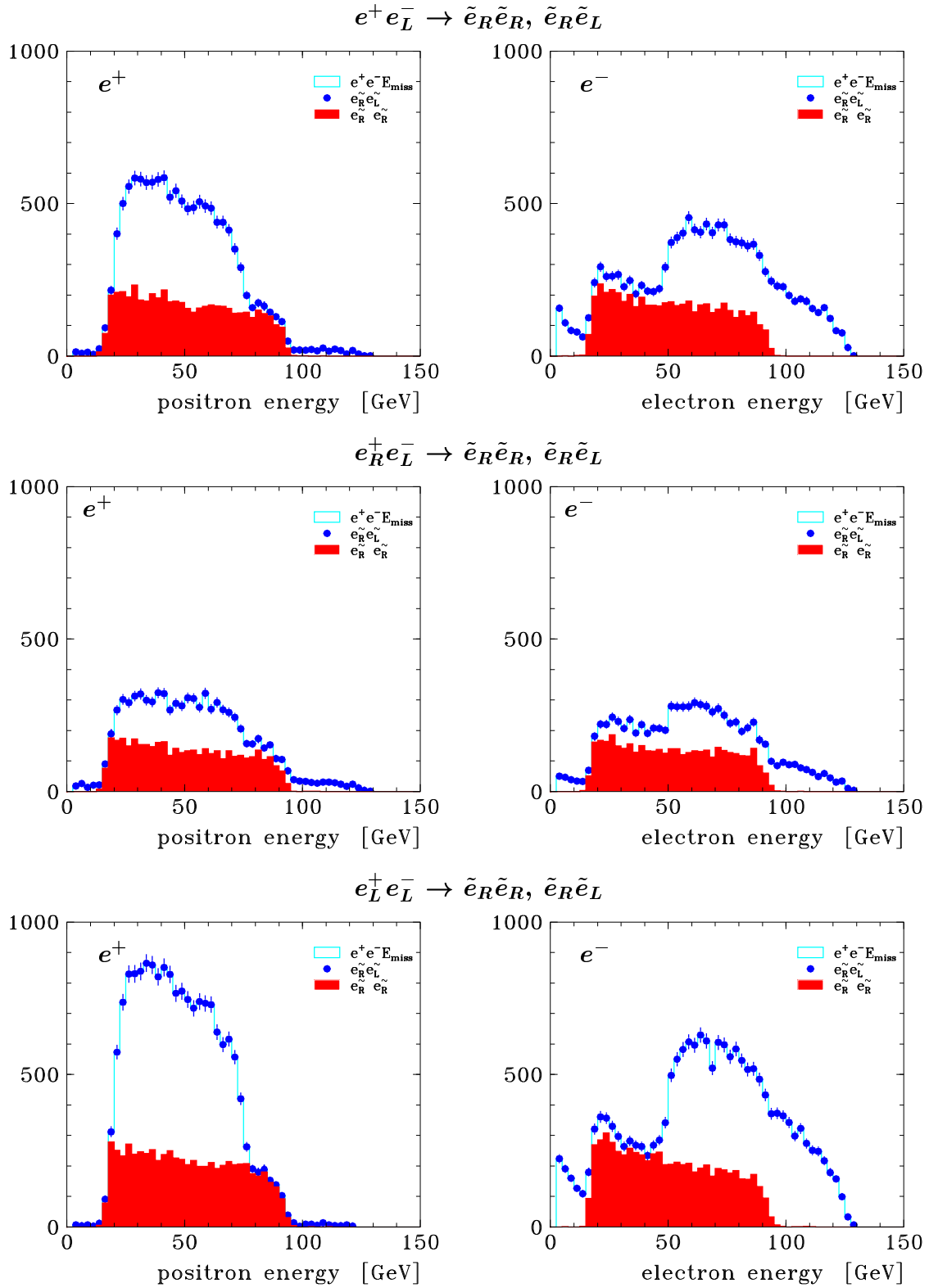


Figure 7:  $e^\pm$  energy spectra from  $e^+e^- \rightarrow \tilde{e}_R\tilde{e}_R + \tilde{e}_R\tilde{e}_L$  production with polarisations  $\mathcal{P}_{e^-} = -0.8$ ,  $\mathcal{P}_{e^+}$  variable for SPS 1a scenario assuming  $\sqrt{s} = 400$  GeV and  $\mathcal{L} = 200 \text{ fb}^{-1}$

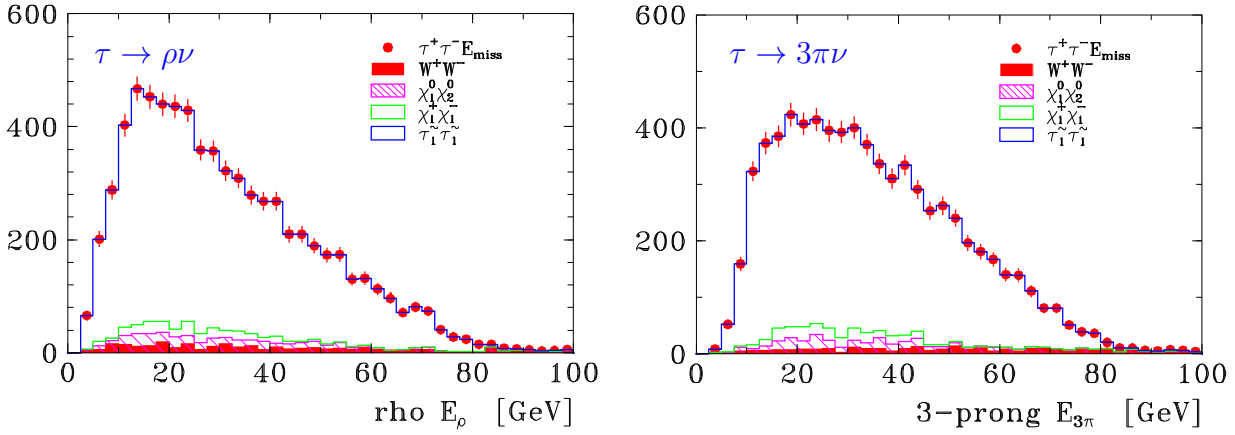


Figure 8: Hadron energy spectra  $E_\rho$  of  $\tau \rightarrow \rho \nu_\tau$  and  $E_{3\pi}$  of  $\tau \rightarrow 3\pi \nu_\tau$  decays from the reaction  $e_L^+ e_R^- \rightarrow \tilde{\tau}_1^+ \tilde{\tau}_1^- \rightarrow \tau^+ \tilde{\chi}_1^0 \tau^- \tilde{\chi}_1^0$  in SPS 1a scenario assuming  $\sqrt{s} = 400$  GeV and  $\mathcal{L} = 200 \text{ fb}^{-1}$

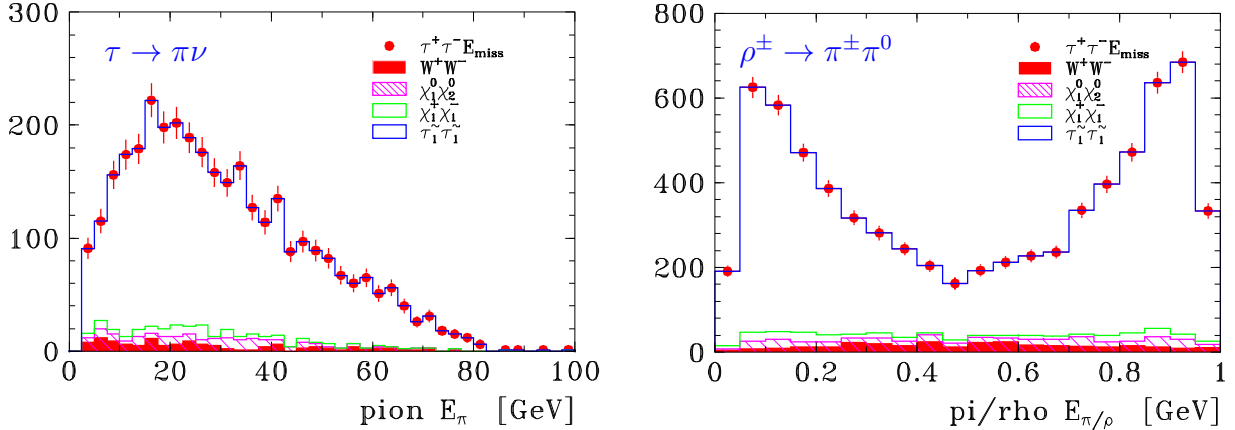


Figure 9: Pion energy spectrum  $E_\pi$  of  $\tau \rightarrow \pi \nu_\tau$  and ratio  $z_\pi = E_\pi/E_\rho$  of  $\tau \rightarrow \rho \nu_\tau$  decays from the reaction  $e_L^+ e_R^- \rightarrow \tilde{\tau}_1^+ \tilde{\tau}_1^- \rightarrow \tau^+ \tilde{\chi}_1^0 \tau^- \tilde{\chi}_1^0$  in SPS 1a scenario assuming  $\sqrt{s} = 400$  GeV and  $\mathcal{L} = 200 \text{ fb}^{-1}$

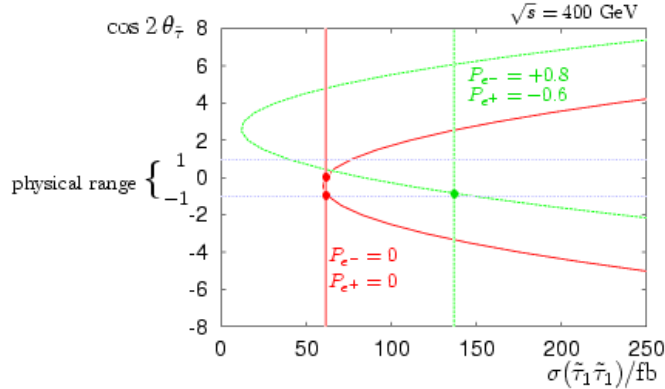


Figure 10: Mixing angle angle  $\cos 2\theta_{\tilde{\tau}}$  versus cross section  $\sigma_{\tilde{\tau}_1 \tilde{\tau}_1}$  at  $\sqrt{s} = 400$  GeV for mSUGRA scenario SPS 1a